Structural characterization and electron-energy-loss spectroscopic study of pulsed laser deposited $LiNbO_3$ films on *a*-sapphire

J. Y. Dai[a] and H. K. Lam
Department of Applied Physics, The Hong Kong Polytechnic University, Hung Hom, Kowloon, Hong Kong, China

Quan Li and J. Wang
Department of Physics, The Chinese University of Hong Kong, Shatin, N.T., Hong Kong, China

H. L. W. Chan and C. L. Choy
Department of Applied Physics, The Hong Kong Polytechnic University, Hung Hom, Kowloon, Hong Kong, China

(Received 3 May 2004; accepted 22 August 2004)

Highly *c*- and *a*-oriented $LiNbO_3$ films were deposited on *a*-sapphire substrates by pulsed laser deposition. The film microstructure and crystal orientation were studied by transmission electron microscopy, and the mechanism forming the different film orientations was interpreted in terms of the adatom energy and oxygen pressures. The electron-energy-loss functions derived from the electron-energy-loss spectra exhibit characteristic energy-loss peaks at about 7.0, 11.0, and 14.0 eV. These peaks correspond to electron transitions from the maximum density of the states in the valence band of O 2*p* to the split conduction band. The dielectric functions of the $LiNbO_3$ films were also derived from the energy-loss function. © *2004 American Institute of Physics*. [DOI: 10.1063/1.1806993]

I. INTRODUCTION

$LiNbO_3$ is a well-known ferroelectric oxide displaying prominent piezoelectric, pyroelectric, electro-optic, photoelastic, and nonlinear optical effects.[1] $LiNbO_3$ has been widely applied for the fabrication of optical waveguide, optical switch, optical modulator, and surface acoustic wave (SAW) devices, and it exhibits important technical value and profound developing prospect in the fields of acoustics, optical communications, integrated optics, and nonlinear optics.[2,3] The deposition of $LiNbO_3$ films and the orientation control of the films on sapphire substrates have been studied by many researchers,[4,5] and it has been shown that for different applications, different orientations of $LiNbO_3$ epitaxial layers may be needed. For example, SAW devices require [0001]-oriented (*c*-oriented) $LiNbO_3$ epitaxy to fully utilize the d_{33} piezoelectric coefficient,[6,7] and the electro-optical modulator devices need the film to be $[11\bar{2}0]$ oriented (*a*-oriented) so that the in-plane piezoelectric property can be utilized to modulate the refractive index.[8] Lee and coworkers have systematically studied the epitaxial deposition of $LiNbO_3$ on *c*- and *a*-plane sapphire substrates.[8,9] Even though the deposition of $LiNbO_3$ on sapphire by pulsed laser deposition (PLD) has been widely studied, surprisingly, the study of the interfacial detail structure and, thus, the understanding of the growth mechanisms are still limited. In this paper, a transmission electron microscopy (TEM) was carried out for a detailed study of the interfacial structure between $LiNbO_3$ films deposited at different oxygen pressures on sapphire substrates, and the orientation control mechanism will be discussed.

For optical device applications, the electronic structure and dielectric function of $LiNbO_3$ films are of fundamental and practical interest. Previously reported electron-energy-loss functions measured by an electron-energy-loss spectrum (EELS) and x-ray photoelectron spectroscope analysis were mainly on single crystals,[10–12] but the energy-loss function of $LiNbO_3$ thin films containing crystal defects and oxygen deficiencies has not been well studied. In this paper, we also report the energy-loss function of the $LiNbO_3$ films on sapphire substrates by means of an EELS-equipped in field-emission TEM. The EELS in-field-emission TEM possesses an excellent spatial resolution, and the dielectric function derived through the Kramers-Kronig transformation reflects the dielectric property from the visible to the soft x-ray region, whereas the ellipsometry measurement only provides the dielectric function from the visible to the ultraviolet range with a finer energy resolution.

II. EXPERIMENTS

The $LiNbO_3$ films were deposited on $10\times10\times0.5$ mm^3 *a*-plane sapphire (Al_2O_3) substrates by PLD with a KrF excimer laser ($\lambda=248$ nm) at a 250 mJ and 5 Hz repetition rate. A $LiNbO_3$ single-crystal target was used in the deposition. The $LiNbO_3$ films were deposited with different oxygen pressures at 600 °C, i.e., 500 mtorr and 100 mtorr, respectively. After deposition, the films were *in situ* annealed at 600 °C for 30 min in an oxygen pressure of 11 torr. The same pressure was maintained until the sample was cooled down to room temperature. The growth rate of

[a]Author to whom correspondence should be addressed: apdaijy@inet.polyu.edu.hk

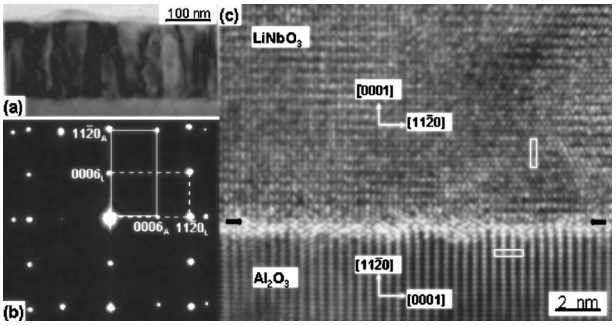

FIG. 1. (a) Cross-section TEM image of a *c*-$LiNbO_3$ on an *a*-sapphire substrate deposited at a 500 mtorr oxygen pressure; (b) the composite diffraction patterns showing the orientation relationship between the $LiNbO_3$ film and sapphire substrate, where "L" and "A" represent $LiNbO_3$ and Al_2O_3, respectively; and (c) the corresponding HREM image of the interface, where the unit cells of $LiNbO_3$ and Al_2O_3 are outlined by the white lines and the interface is indicated by the arrow.

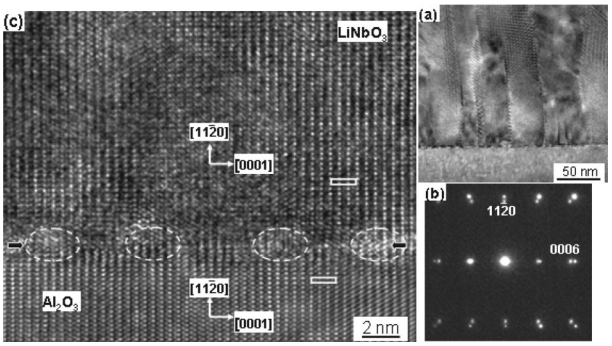

FIG. 2. (a) Cross-section TEM image of an *a*-$LiNbO_3$ on an *a*-sapphire substrate deposited at a 100 mtorr oxygen pressure; (b) the composite diffraction patterns showing the orientation relationship between the $LiNbO_3$ film and sapphire substrate, where the labeled (0006) and $(11\bar{2}0)$ diffractions are for $LiNbO_3$ and Al_2O_3; and (c) the corresponding HREM image of the interface, where the unit cells of $LiNbO_3$ and Al_2O_3 are outlined by the white lines and the interface is indicated by the arrow. The strained areas due to the interfacial dislocations are indicated by the white dot circles.

the films is about 0.5 nm/s and the film thicknesses are about 200 nm. The cross-section TEM study of $LiNbO_3/Al_2O_3$ was carried out on a field-emission electron microscopy. The energy-loss function and dielectric function of the $LiNbO_3$ films were obtained from the EELS using the Kramers-Kronig transformation.[13]

III. RESULTS AND DISCUSSION

A. Interfacial structure

Figure 1(a) shows a cross-section TEM image of *c*-$LiNbO_3$ on an *a*-sapphire substrate deposited at a 500 mtorr oxygen pressure and the diffraction pattern, as shown in Fig. 1(b), illustrating the orientation relationship between the $LiNbO_3$ film and the sapphire substrate, i.e., $(0001)_{LiNbO_3} \| (11\bar{2}0)_{Al_2O_3}$ and $[01\bar{1}0]_{LiNbO_3} \| [01\bar{1}0]_{Al_2O_3}$. The film exhibits a columnar and epitaxial growth feature with a grain size of about 100 nm. Figure 1(c) is the corresponding high-resolution electron microscopy (HREM) image showing the interfacial structure. It can be seen that the interface is free from interfacial reaction, and the interface is sharp even with the presence of a large number of misfit dislocations at the interface due to the lattice mismatch.

Figure 2(a) is a TEM image showing an *a*-$LiNbO_3$ on an *a*-sapphire substrate grown at 100 mtorr. The corresponding orientation relationship between the film and substrate is illustrated by the composite-electron diffraction pattern, as shown in Fig. 2(b), i.e., $(11\bar{2}0)_{LiNbO_3} \| (11\bar{2}0)_{Al_2O_3}$ and $[01\bar{1}0]_{LiNbO_3} \| [01\bar{1}0]_{Al_2O_3}$. Again, from the corresponding HREM image, as shown in Fig. 2(c), it can be seen that the interface is sharp and free from interfacial reaction. The misfit dislocations exhibit a periodic feature with a mean distance of 5.6 nm, and the induced strains at the interface can be clearly seen.

It is worthy to note that some areas in the $LiNbO_3$ film deposited at a 100 mtorr oxygen pressure show coexistence of the *a*- and *c*-orientations, as shown in Fig. 3. The percentage of the *c*-oriented grains is about 10%. This suggests that the interfacial mismatch energies between the *a*- and *c*-oriented $LiNbO_3$ with an *a*-sapphire is small and may be tolerated by other factors such as oxygen pressure, laser beam energy, etc. The film orientation does not change as the film thickness increases, but we noticed that some small *c*-oriented grains were finally "eaten-up" by the neighboring *a*-oriented domains. This suggests that the *a*-oriented grains may grow faster than the *c*-oriented grains at a low oxygen pressure. Consider also the work reported earlier by Lee and co-workers,[8,9] where a much lower oxygen pressure resulted only in the *a*-orientated growth of the $LiNbO_3$ film; we believe that it should be a continuous change of the film growth orientation as the oxygen pressure changes.

The results turned out that oxygen pressure is the key parameter that affects the growth orientation of $LiNbO_3$ on sapphire substrates. A higher oxygen pressure favors the *c*-axis $LiNbO_3$ growth and a lower oxygen pressure favors the *a*-axis growth. Lee and co-workers have ascribed this to the different atomic arrangements of the oxygen layers in the *c*- and *a*-oriented $LiNbO_3$.[9] However, our results showed that

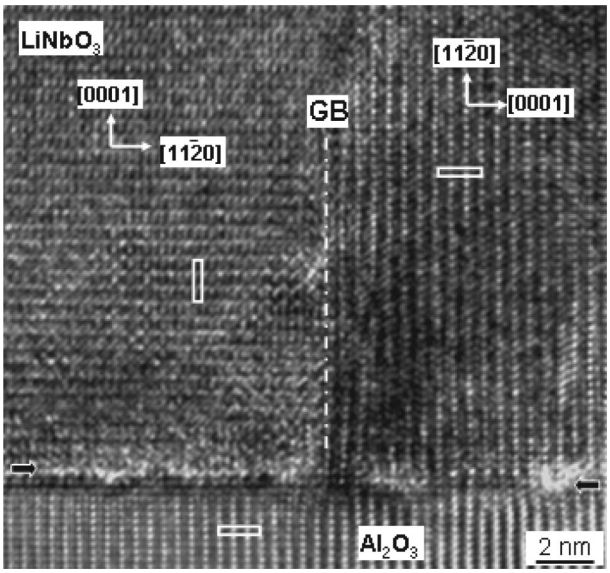

FIG. 3. HREM image of the $LiNbO_3$ film on an *a*-sapphire substrate deposited at a 100 mtorr oxygen pressure showing coexistence of the *a*- and *c*-oriented $LiNbO_3$. The white dot line indicates the grain boundary between the *a*- and *c*-oriented $LiNbO_3$.

this rule was broken when the laser energy changed. For example, when the laser fluence was reduced from 5 to 3 J/cm^2, the same low oxygen pressure (100 mtorr) still resulted in the *c*-$LiNbO_3$ growth. We believe that the adatom energy is an important factor that controls the crystal orientation of the $LiNbO_3$ films during the nucleation stage, and the oxygen pressure also affects the growth orientation through changing the adatom energy. In fact, both a higher oxygen pressure and a lower laser power result in a lower adatom energy; therefore, the adatom energy should play the most important role in controlling the film growth orientation.

The lattice similarity between $LiNbO_3$ and sapphire determines that the interfacial energy of an *a*-$LiNbO_3$/*a*-sapphire is lower than that of a *c*-$LiNbO_3$/*a*-sapphire. However, another competition factor is the nucleation surface free energy. The Gibbs free energy has been thought to play an important role in the nucleation stage, which directly affects the growth orientation of the films. A model based on the change of the Gibbs free energy in forming a single-crystal nucleus has been proposed to interpret the *c*-oriented $LiNbO_3$ growth on an amorphous SiO_2.[6] We believe that when the oxygen pressure is higher, its rapid quenching effect results in a lower adatom energy, and the lower adatom energy makes it difficult to overcome the energy barrier to allocate to the correct lattice sites and, thus, the surface free energy becomes a dominant factor in controlling the growth orientation of the $LiNbO_3$ nucleus. Since $LiNbO_3$ has the hexagonal structure, the (0001) lattice plane has the largest atomic density and the lowest surface free energy thus grows preferentially along the *c* axis on the amorphous substrates. Therefore, if the difference of the lattice mismatches between the *c*- and *a*-oriented $LiNbO_3$ with an *a*-sapphire is small, in fact it is true,[9] the *c*-oriented $LiNbO_3$ will be a preferred orientation when the adatom energy is relatively low. This interpretation matches the reported results by Lee and co-workers,[9] where the higher and lower oxygen pressures resulted in the *c*- and *a*-oriented $LiNbO_3$ films grown on *c*-sapphire substrates, respectively. Based on the adatom energy understanding, we believe that the growth orientation of the $LiNbO_3$ films on a *c*-sapphire substrate may also be controlled by altering the laser fluence. This is desirable for further studies.

B. Electron-energy-loss function and electronic structure

The EELS spectra of the *a*- and *c*-oriented $LiNbO_3$ films were obtained using the diffraction mode at zero-momentum transfer. The energy-loss functions of these two differently oriented $LiNbO_3$ films after the multiple-scattering corrections were obtained from the raw EELS spectra, and it turns out that the general shapes of the spectra are the same, and there is no significant difference to be noticed. Figure 4 represents a typical energy-loss function obtained from the $LiNbO_3$ films. Based on the first-principle calculation by Kohiki *et al.*[10] and the experimental results reported by Kasper and Hüfner,[11] the electron-energy losses of about 7.0, 14.0, and the small shoulder at 11.0 eV can be attributed to the

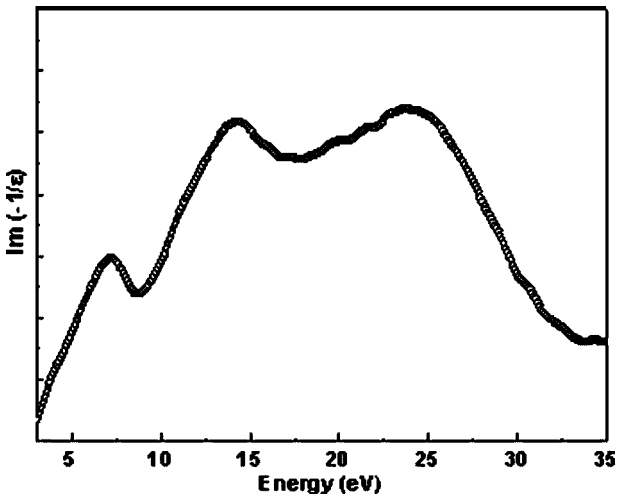

FIG. 4. (a) Represented energy-loss function of the $LiNbO_3$ films after the multiple scattering corrections from the raw energy-loss spectra.

electron transitions from the maximum density of the states in the valence band to the split conduction band, where the valence band is predominantly of O 2*p* character and the conduction band contains Nb *d* and *s*-*p* states.

Kasper and Hüfner have reported that the Li or O deficiency induced a reduction of Nb^{5+} to Nb^{4+} and resulted in an energy-loss peak at 5.2 eV. The fact that such a peak was absent in our PLD-deposited $LiNbO_3$ films suggests that the $LiNbO_3$ films are well crystallized without the significant oxygen and Li deficiencies. The peak at 24 eV in the energy-loss function is attributed to a plasmon peak.

Figures 5(a) and 5(b) show the real and imaginary parts

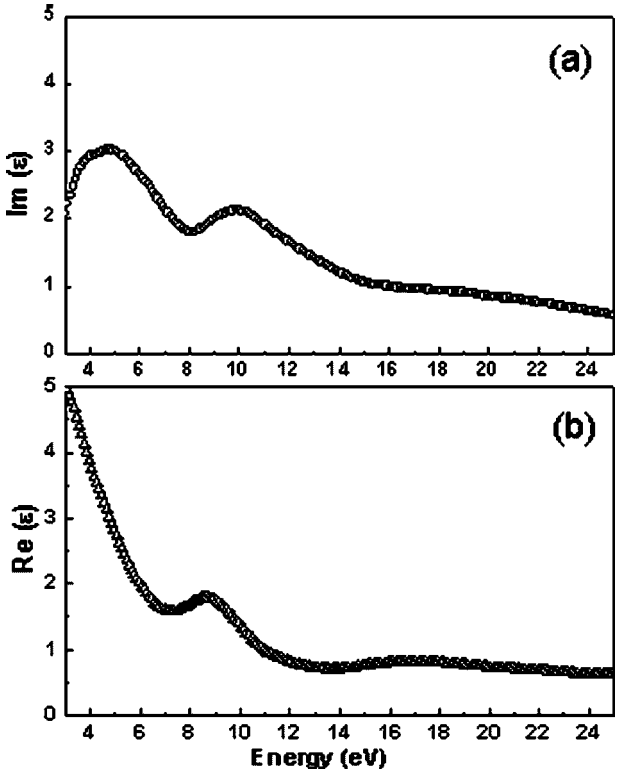

FIG. 5. Dielectric function of the $LiNbO_3$ films derived by using the Kramers-Kronig transformation: (a) Im(ε) and (b) Re(ε).

of the dielectric function derived from the loss function by using the Kramers-Kronig transformation. The peaks in $\mathrm{Im}(\varepsilon)$ correspond to the joint density of the states in the valence and conduction bands, and the broad peaks at 4.0–5.0 eV and 9.0–10.0 eV match fairly well with the first-principle calculation result as reported by Kohiki *et al.*[10]

IV. CONCLUSION

Highly *c*- and *a*-oriented $LiNbO_3$ films were deposited on *a*-sapphire substrates by PLD. The film microstructure and crystal orientations were studied by TEM, and the mechanism forming the different film orientations was interpreted in terms of the adatom energy and oxygen pressure. The energy-loss functions and dielectric functions derived from the EELS exhibit characteristic peaks that are similar to bulk $LiNbO_3$ single crystals.

ACKNOWLEDGMENTS

This work was partially supported by the Hong Kong RGC grant (Grant No. B-Q553) and also an internal grant from the Hong Kong Polytechnic University (Grant No. G-YD55).

[1]X. C. Wang, Z. Ye, and J. He, Int. J. Mod. Phys. B **16**, 4343 (2002).
[2]Y. Shibata, K. Kaya, and K. Akashi, Appl. Phys. Lett. **61**, 1000 (1992).
[3]X. Yang, X. L. Wu, and W. W. Xue, Appl. Phys. Lett. **82**, 4456 (2003).
[4]D.-W. Kim, S.-H. Lee, and T. W. Noh, Mater. Sci. Eng., B **56**, 251 (1998).
[5]G. Balestrino, S. Martellucci, and P. G. Medaglia, Appl. Phys. Lett. **78**, 1204 (2001).
[6]J. H. He and Z. Z. Ye, Chinese Science Bulletin **48**, 2290 (2003).
[7]Y. Shibata, K. Kaya, and K. Akashi, J. Appl. Phys. **77**, 1498 (1995).
[8]S. H. Lee, T. W. Noh, and J.-H. Lee, Appl. Phys. Lett. **68**, 472 (1996).
[9]S. H. Lee, T. K. Song, T. W. Noh, and J.-H. Lee, Appl. Phys. Lett. **67**, 43 (1995).
[10]S. Kohiki, M. Arai, H. Yoshikawa, and S. Fukushima, Phys. Rev. B **57**, 14572 (1998).
[11]L. Kasper and S. Hüfner, Phys. Lett. **81**, 165 (1981).
[12]W. Y. Ching, Z. Q. Gu, and Y. N. Xu, Phys. Rev. B **50**, 1992 (1994).
[13]R. F. Egerton, *Electron Eenergy-Loss Spectroscopy in the Electron Microscope* (Plenum Press, New York, 1996).